

**P. Blanc-Benon, D. Marx**  
**NONLINEAR EFFECTS IN A STANDING WAVE THERMOACOUSTICS**  
**REFRIGERATOR**

Laboratoire de Mécanique des Fluides et d'Acoustique  
UMR CNRS 5509, Ecole Centrale de Lyon, 69134 Ecully Cedex, France  
Email: Philippe.Blanc-Benon@ec-lyon.fr

*In thermoacoustic refrigerators, the acoustic energy provided by an acoustic source is used to pump heat from a cold reservoir. Such refrigerators may possibly be miniaturized, offering an application to microelectronic refrigeration. The knowledge of temperature and flow fields in the microchannels and at the edges of the stack plates becomes an increasingly important issue in the design of heat exchangers for thermoacoustic engines. On these topics we have developed numerical simulations and conducted experiments in a resonant standing wave thermoacoustic refrigerator model. In this paper the full compressible Navier-Stokes equations are solved numerically, and the flow and heat transfer around a 2-D stack plate immersed in an acoustic standing wave are computed. Non-harmonic temperature variations are found and are explained using the results of a former nonlinear analysis. The effects of the acoustic Mach number and geometrical parameters on refrigerator performance are investigated.*

**1. Introduction**

Thermoacoustic refrigerators have been developed since the early 1980's [1]. They offer some advantages, among which, the use of environmentally benign fluids, and a possible miniaturization, with an application to microelectronic refrigeration [2]. The thermoacoustic refrigerator considered in the following is shown in Fig. 1. It consists mainly of three parts: a half-wavelength resonator, an acoustic source, and a stack of tightly-spaced parallel plates. The acoustic source and resonator create an acoustic standing wave of high amplitude. The interaction of this wave with the stack of plates results in a heat flux along the stack, parallel to the resonator axis. To design and predict performance of thermoacoustic refrigerators, the most widely used tool is the standard "linear theory" [1]. In the frame of this theory, the governing equations (i.e. the full two-dimensional Navier-Stokes equations) are first linearized, and then space-averaged over the resonator cross section, that is over the y-direction. This provides a one-dimensional model in the x-direction, which takes into account the temperature gradient along the stack, as well as viscous and thermal boundary layers. Unfortunately this theory can not take into account a large amount of phenomena. In particular, nonlinear effects, as well as two-dimensional flows are not included in the model. However vortical motions at the extremities of the stack plates have been observed both experimentally [3] and numerically [4,11]. Acoustic nonlinear effects consist of acoustic streaming [5,6,7] and waveform distortions. Nonlinear effects have sometimes been alluded to explain the divergences between experimental or numerical results and linear theory predictions [4,8]. To include all physical phenomena involved in thermoacoustic heat pumping (boundary layers, nonlinear acoustic, heat transfer,

temperature gradient, two-dimensional flow), a numerical solver was developed at ECL. A few numerical studies of thermoacoustic phenomena have already been performed [4,9]. The present simulation solver is based on the solution of the two-dimensional compressible and unsteady Navier-Stokes equations. It allows the simulation of the flow and heat transfer in the vicinity of a stack plate in the presence of an acoustic standing wave of high amplitude.

## 2. Numerical models

The numerical simulation of the whole refrigerator shown in Fig.1 would be far too costly in term of computational time [10]. Hence the computational domain has to be a small part of the whole refrigerator, and is named CD in Fig.1. This domain is shown in Fig.2. Taking advantage of the periodicity of the stack, which usually includes a large number of plates, with no differences from one plate to another, CD includes only a half-plate of the stack. As a result, the height of the domain,  $y_0$ , is half plate spacing in the stack. This distance is usually a few times the thermal boundary layer thickness,  $\delta_\kappa$ , defined by:  $\delta_\kappa = \sqrt{\frac{\kappa}{\pi f}}$ , where  $f$  is

the frequency, and  $\kappa$  is the thermal diffusivity defined by  $\kappa = K / \rho c_p$ . The fluid thermal conductivity is  $K$ ,  $\rho$  is its density, and  $c_p$  is its isobaric specific heat. For usual fluids  $\delta_\kappa$  is not very different from the viscous boundary layer thickness,  $\delta_\nu$ , another important quantity in thermoacoustics, defined in the same manner as  $\delta_\kappa$ , but replacing  $\kappa$  by  $\nu$ , where  $\nu$  is the dynamic viscosity. The actual half-thickness of the plate,  $E$ , may (Fig 2a), or may not (Fig 2b), be taken into account. This depends on the model equation for the plate. The length of the plate is  $L$ . Its position in the resonator is given by  $kx_s$ , where  $x_s$  is the plate center position (see Fig. 1), and  $k = 2\pi / \lambda$  is the wave number, where  $\lambda$  is the wave length. Also to be noticed, CD includes the resonator rigid end, but it does not include the acoustic source. The difficult modelling of the source is thus avoided by using a characteristics-based method in section  $S_{inout}$ . A standing wave is created in the computational domain in the following manner: an incident traveling wave is introduced into the computational domain through section  $S_{inout}$ , which is reflected at the rigid end of the resonator. The reflected traveling wave leaves the domain through  $S_{inout}$ . The superimposition of the incident and reflected waves results in the standing wave that is needed. To further reduce the computational time, the frequency had a high value,  $f=20$  kHz. Making this choice reduces the length of the computational domain compared to the boundary layers thicknesses, and hence compared to the spatial mesh size [10]. The value for  $f$  is higher than the few hundreds hertz used in most experiments. Nevertheless a 5 kHz refrigerator has already been tested [2], which corresponds to miniaturization goals. The choice of a high frequency does not actually affect the physics of thermoacoustic

heat pumping. The wavelength corresponding to the chosen frequency takes the value  $\lambda = c_0/f = 17\text{mm}$ , where  $c_0$  is the speed of sound.

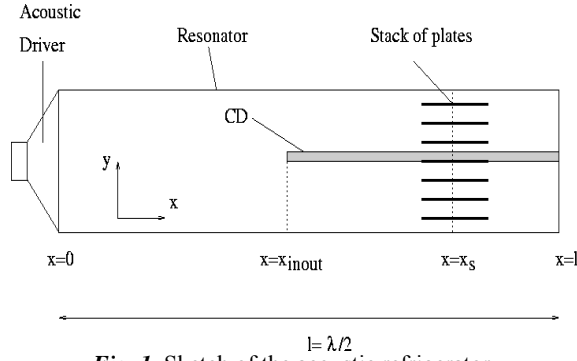


Fig. 1. Sketch of the acoustic refrigerator.

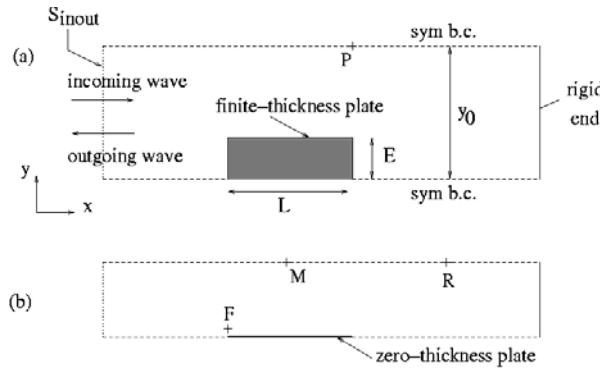


Fig 2. Computational domain CD : with (a) a finite-thickness plate, or with (b) a zero-thickness plate.

The governing equations for the fluid are the state equation, the continuity equation, the two-dimensional compressible Navier-Stokes equations, and the energy conservation equation :

$$p = \rho r T, \quad (1)$$

$$\frac{\partial \rho}{\partial t} + \nabla \cdot (\rho \mathbf{u}) = 0, \quad (2)$$

$$\frac{\partial (\rho \mathbf{u})}{\partial t} + \nabla \cdot (\rho \mathbf{u} \mathbf{u}) + \nabla p = \nabla \tau, \quad (3)$$

$$\frac{\partial T}{\partial t} + \mathbf{u} \cdot \nabla T + (\gamma - 1) T \nabla \cdot \mathbf{u} = \frac{(\gamma - 1)}{\rho r} (\Phi + \nabla \cdot (K \nabla T)), \quad (4)$$

where  $p$  and  $T$  are respectively the pressure, and the temperature of the fluid. The velocity vector is  $\mathbf{u}=(u,v)$ . The stress tensor,  $\boldsymbol{\tau}$ , has the following components:

$$\tau_{xx} = \frac{4}{3}\mu \frac{\partial u}{\partial x} - \frac{2}{3}\mu \frac{\partial v}{\partial y}, \quad \tau_{yy} = \frac{4}{3}\mu \frac{\partial v}{\partial y} - \frac{2}{3}\mu \frac{\partial u}{\partial x}, \quad (5)$$

$$\tau_{xy} = \tau_{yx} = \mu \left( \frac{\partial u}{\partial y} + \frac{\partial v}{\partial x} \right). \quad (6)$$

The viscous dissipation,  $\Phi$ , is defined by  $\Phi = \boldsymbol{\tau} : \nabla \mathbf{u}$ . The fluid shear viscosity is  $\mu$ . The gas constant is  $r$ , the ratio of specific heats is  $\gamma$ . Fluid is taken to be air, considered as a perfect gas, in ambient conditions. Its density, temperature, and pressure at rest are  $\rho_0=1.2 \text{ kg m}^{-3}$ ,  $T_0=298 \text{ K}$ , and  $p_0=100 \text{ kPa}$ , respectively. In the following, for any variable,  $G$ , the notation  $G = G_0 + G'$  will be used, where  $G_0$  is the value at rest, and  $G'$  is the fluctuation in the presence of the acoustic wave. The following values are taken:  $r=287 \text{ J K}^{-1} \text{ kg}^{-1}$ ,  $\gamma=1.4$ ,  $K=0.025 \text{ W K}^{-1} \text{ m}^{-1}$ , and  $\mu=1.8 \cdot 10^{-5} \text{ Pa s}$ . For the plate, two different equations for the conservation of energy were used. For a finite-thickness plate (Fig. 2a), the equation is the two-dimensional heat equation:

$$\rho_s c_s \frac{\partial T_s}{\partial t} = K_{sx} \frac{\partial^2 T_s}{\partial x^2} + K_{sy} \frac{\partial^2 T_s}{\partial y^2}, \quad (8)$$

where  $T_s$  is the temperature of the plate,  $\rho_s$  is its density, and  $c_s$  is its calorific capacity. As can be seen in Eq. (8) the thermal conductivity of the plate in the  $x$ -direction,  $K_{sx}$ , is taken to be different from its thermal conductivity in the  $y$ -direction,  $K_{sy}$ :  $K_{sx}$  takes a realistic value, whereas  $K_{sy}$  takes a much higher value than  $K_{sx}$ . This allows reaching a steady state in the plate in a shorter computational time. The solid is made of Mylar:  $\rho_s=1350 \text{ kg m}^{-3}$ ,  $K_{sx}=0.14 \text{ WK}^{-1} \text{ m}^{-1}$ ,  $c_s=1300 \text{ JK}^{-1} \text{ kg}^{-1}$ . For the transversal conductivity,  $K_{sy}=1000 K_{sx}$ . Eq. (8) is a realistic model, but for a reduced complexity of the code, as well as for a reduced computational time, a zero-thickness model has also been used. It consists of neglecting the geometrical thickness of the plate (Fig. 2b). Also, for even more simplicity, this zero-thickness plate is supposed to be isothermal; its temperature is uniform and takes the value  $T_0$ . Such a model is simplified, but it is sufficient to get a thermoacoustic effect, that is a heat pumping along the plate, in the fluid above it. It has already been used by Cao et al. [9]. Some boundary conditions still need to be provided: on the plate surface, the continuity of both the temperature ( $T=T_s$ ) and the heat flux is enforced for a finite-thickness plate model. For the zero-thickness plate model, only the temperature continuity needs to be enforced, it is simply equivalent to  $T=T_s=T_0$ . Also, on the plate, no-slip boundary conditions are enforced. On the top and bottom boundaries of CD, symmetrical conditions are used. On the rigid end of the resonator, a simplified adiabatic condition is enforced. The governing equations are discretized on a two-

dimensional Cartesian grid. In the vicinity of the plate, the mesh is uniform and the mesh size is such that there are at least 8 grid points per viscous boundary layer. Past the plate, the mesh is stretched in the x-direction, up to 20 times this value. The equations are solved using a 4<sup>th</sup> order finite differences scheme for spatial derivatives and a four order Runge-Kutta scheme for time integration. High order spatial filtering is also used to suppress grid to grid oscillations. More details about the simulation may be found elsewhere [10,11,15].

### 3. Results

First, nonlinear behaviors were investigated. One important parameter in this investigation is the acoustic Mach number,  $M_a$ , defined by:  $M_a = u_A/c_0$ , where  $u_A$  is the maximum amplitude of the velocity in the resonator. The acoustic Mach number is a measure of the strength of the acoustic standing wave. In thermoacoustics, the drive ratio,  $Dr$ , which is the ratio of the maximum acoustic pressure in the resonator to the mean pressure, is often used. We have the simple relation  $M_a = Dr/\gamma$ . It is generally accepted that nonlinear effects appear when  $M_a$  is above around 2% [4,8], although the nature of the involved nonlinearities is indeed not very clear. In the present investigation, the zero-thickness isothermal model was used for the plate. The values of the simulation parameters are the following:  $L/\lambda = 1/40$ ,  $\delta_x/y_0 = 0.37$ ,  $kx_s = 2.13$ . A large range for the Mach number (up to 8%) was used. As a nonlinear behavior generally implies harmonics generation, the time variations of velocity and temperature were first recorded at several points of the computational domain. The temperature time variation at point M (see Fig 2b) is shown in Fig. 3 for different values of the Mach number. Time is made dimensionless using the acoustic period,  $\tau$ . At low Mach numbers,  $M_a < 4\%$ , the temperature variation is sinusoidal. For a high enough Mach number,  $M_a = 8\%$ , the temperature variation is not sinusoidal anymore, indicating the presence of harmonics, and showing the importance of nonlinear effects. The time variation of the velocity at point M, for different Mach numbers is shown in Fig. 4. As can be seen, the velocity variation, unlike the temperature variation, remains sinusoidal, even for the highest value of the Mach number,  $M_a = 8\%$ . The temperature time variation was also recorded at point F of the domain (see Fig. 2b), located just above the cold extremity of the plate. This variation is shown in Fig. 5, for different values of the Mach number. Even for the lowest Mach numbers,  $M_a < 4\%$ , the temperature variation is not sinusoidal. At the highest Mach number,  $M_a = 8\%$ , the distortion of the temperature waveform at point F is much more pronounced than that at point M (see Fig. 3). Again, unlike the temperature variation, the velocity variation at point F (not shown), remains sinusoidal for the whole Mach number range. Finally far from the stack region (point R), the temperature and velocity waveforms both remain sinusoidal. Hence, in the stack region (only), the term  $\mathbf{u} \cdot \nabla T + (\gamma - 1)T \nabla \cdot \mathbf{u}$  in Eq. (4) for

temperature has a much more important effect than the nonlinear term  $\nabla \cdot (\rho \mathbf{u} \mathbf{u})$  in Eq. (3) for velocity. Importantly, in the linear theory [1], the nonlinear term in Eq. (4) is linearized, and thus becomes:  $\mathbf{u} \cdot \nabla T_m + (\gamma - 1) T_m \nabla \cdot \mathbf{u}$ , where  $T_m$  is the mean temperature.

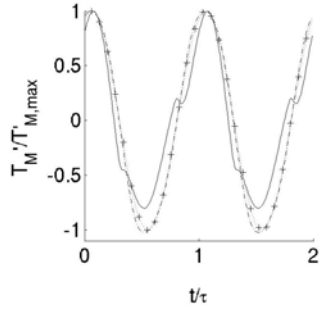


**Fig. 3.** Temperature variation,  $T'_M$ , at point M, divided by the maximum value of the temperature fluctuation,  $T'_{M,max}$ , at point M, for different values of the Mach number: +++ Ma=0.5%; ··· Ma=2%; - - - Ma=4 %; — Ma=8%.

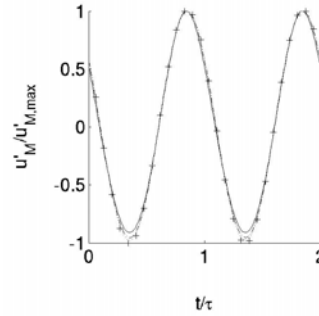


**Fig. 4.** Velocity variation,  $u'_M$ , at point M, divided by the maximum value of the velocity fluctuation,  $u'_{M,max}$ , at point M, for different values of the Mach number: +++ Ma=0.5%; ··· Ma=2%; - - - Ma=4 %; — Ma=8%.

The results above show that this linearization may indeed be not fully correct at high driving amplitudes. The results above also show that the waveform distortion is much more important at the edges of the plate, than in its center. These results may be explained by considering a nonlinear analysis by Gusev et al. [12]. Considering a non-viscous problem, these authors show that the nonlinear convective term in the energy equation is responsible for temperature harmonics generation at the edges of the plate, in a region of length  $4d_a$ , where  $d_a$  is the particle displacement amplitude, defined by:  $d_a = \frac{u_a}{2\pi f}$ . In this equation  $u_a$  is

the velocity amplitude. For a standing wave in the resonator, the value of  $d_a$  is given by:  $d_a = M_a \frac{\lambda}{2\pi} \sin(kx_s)$ . The region of nonlinear behavior for the

temperature, which may be deduced from the work of Gusev et al., is shown in Fig. 6a. It corresponds to the case when the particle displacement is small. For a fixed geometry,  $d_a$  is small when  $M_a$  is small. As can be seen in Fig. 6a, even for a small  $d_a$ , point F is located in the nonlinear area, while point M is not in the area. This explains why, at low Mach numbers, the temperature variation at point F presents harmonics, but not the variation at point M. When the Mach number increases, the particle displacement increases as well, and Fig. 6b has to be considered. In Fig. 6b, the particle displacement is big enough so that the

nonlinear area extends up to the plate center, so that both points F and M are now in the nonlinear area. This explains why the temperature variation presented some harmonics at both points when the Mach number was high enough. Actually, the nonlinearity of temperature can be observed at point M as soon as  $L=4d_a$ , that is

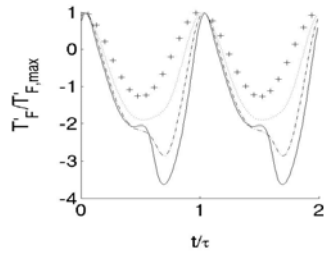


**Fig. 5 :** Temperature variation,  $T_F$  at point F, divided by the maximum value of the temperature fluctuation,  $T_{F,max}$ , for different values of the Mach number: +++ Ma=0.5%; ··· Ma=2%; - · - Ma=4 %; — Ma=8%.

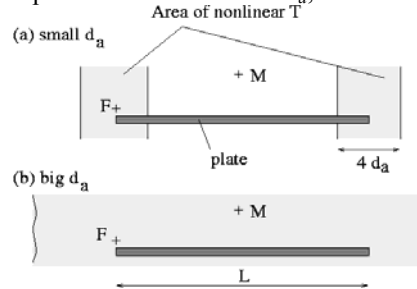


**Fig. 6 :** Area in which the temperature variation of T has a nonlinear behaviour, in two cases: (a) The acoustic displacement amplitude,  $d_a$ , is small; (b) the particle displacement amplitude,  $d_a$ , is large.

when:  $L = 4M_a \frac{\lambda}{2\pi} \sin(kx_s)$ . Therefore whether the temperature variation above the plate is expected to be non-harmonic depends on three parameters: the Mach number, the position of the plate, and the length of the plate. The effect of Mach number has just been discussed. Moreover it was indeed observed in a previous

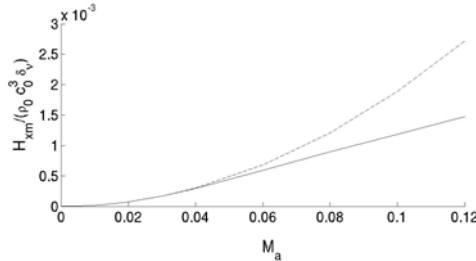


**Fig. 7** Mean heat flux  $H_{xm}$  carried along the plate as a function of the Mach number: — calculated flux; ----  $M_a^2$  fitting at low values of  $M_a$ .

study [10] that for a fixed position of the plate, the Mach number at which the temperature variation at point M becomes non-harmonic decreases as the plate length decreases. It was also noticed that for a fixed length of the plate, the Mach number at which the temperature variation at point M becomes non-harmonic decreases as the plate is pushed toward the velocity antinode (because then  $\sin(kx_s)$  increases, which means that  $M_a$  decreases, as  $L$  is fixed). The analysis of Gusev et al. [12], is confirmed by the present simulations. In particular, the analysis of Gusev et al. dealt with a non-viscous fluid. It appears that taking into

account the viscosity in the present calculations does not prevent the apparition of nonlinear temperature harmonics, nor does it create any velocity harmonic. One consequence of taking viscosity into account is that the velocity variation is canceled on the plate due to no-slip boundary conditions. This effect may be compared to the thermal effect of the plate, which is to cancel the fluid temperature variation on the plate surface (due to the large specific heat of the plate). Despite this, the velocity and temperature have different behaviors because momentum is not exchanged between the plate and the fluid, while thermal energy is. And of course this energy exchange is important due to the presence of thermoacoustic heat pumping. The effect of the temperature waveform distortions on the performance of the refrigerator is shown in Fig. (7), which shows the mean thermoacoustic heat flux carried along the plate,  $H_{xm}$ , plotted as a function the Mach number. It appears that at low Mach numbers,  $M_a < 4\%$ , the heat flux varies as  $M_a^2$ , as is expected from the linear theory. For higher Mach numbers however, when temperature harmonics are present, the heat flux varies as  $M_a$  only. Thus, the apparition of nonlinearity should be avoided, making use  $L=4d_a$ . All the results presented above were obtained using a zero-thickness plate and an isothermal model, for which more results could be collected. However, similar results were obtained when a finite-thickness plate governed by a heat equation was used.

#### 4. Conclusion

The flow and heat transfer in the vicinity of the plate of a thermoacoustic refrigerator stack have been computed. Some temperature waveform distortions have been observed at high Mach numbers and their presence has been explained using the results provided by a former nonlinear analysis. In particular, it has been shown that the nonlinear convective term of the energy equation has a more important effect in thermoacoustics than the nonlinear convective term of the momentum equation. When present, temperature harmonics reduce the thermoacoustic heat pumping by the plate. Results have been presented using an isothermal zero-thickness plate model, but equivalent results were obtained using a finite-thickness plate governed by a heat equation. The effects described here, nonlinear effects, and complex flow structures and heat transfers, are not taken into account in the frame of the usual linear theory. It is believed that these phenomena may have an important effect on the performance of an acoustic refrigerator, especially if it is driven at high amplitudes.

#### 5. Acknowledgments

The authors acknowledge the Délégation Générale pour l'Armement for its financial support, and IDRIS CNRS for providing computing time.

#### REFERENCES

1. Swift, G. W., 1988, Thermoacoustic engines, *J. Acous. Soc. Am.*, **84**, n. 4, pp. 1145-1180.

2. Symko, O. G., Abdel-Rahman, E., Kwon, Y. S., Emmi, M., and Behunin, R., 2004, Design and development of high-frequency thermoacoustic engines for thermal management in microelectronics, *Microelectronics Journal*, **35**, pp. 185-191.
3. Duffourd, S., 2001, Réfrigérateur thermoacoustique: études analytiques et expérimentales en vue d'une miniaturisation, PhD thesis, ECL 2001-06, Ecole Centrale de Lyon.
4. Worlikar, 1997, A., Numerical simulation of thermoacoustic refrigerator, PhD thesis, The Johns Hopkins University, Baltimore.
5. Waxler, R., 2001, Stationary velocity and pressure gradients in a thermoacoustic stack, *J. Acoust. Soc. Am.*, **109**, 2739--2750.
6. Bailliet, H. A., Gusev, V., Raspet, R., and Hiller, R. A., 2001, Acoustic streaming in closed thermoacoustic devices", *J. Acoust. Soc. Am.*, **110**, pp. 1808--1821.
7. Hamilton, M. F., Ilinskii, Y. A., and Zabolotskaya, E. A., 2003, Acoustic streaming generated by standing waves in two-dimensional channels of arbitrary width, *J. Acoust. Soc. Am.*, **113**, pp. 153--160.
8. Poese, M. E., and Garrett, S. L., 2000, Performance measurements on a thermoacoustic refrigerator driven at high amplitudes, *J. Acous. Soc. Am.*, **107**, pp. 2480-2486.
9. Cao, N., Olson, J., Swift, G. W., and Chen, S., 1996, Energy flux density in a thermoacoustic couple, *J. Acoust. Soc. Am.*, **99**, pp. 3456-3464.
10. Marx, D., and Blanc-Benon, Ph., 2004, Numerical simulation of the stack-heat exchangers coupling in a thermoacoustic refrigerator. *AIAA Journal*, **42**, pp.1338-1347.
11. Marx, D., 2003, Simulation numérique d'un réfrigérateur thermoacoustique, PhD Thesis, ECL 2003-34, Ecole Centrale de Lyon.
12. Gusev, V., Lotton, P., Bailliet, H., Job, S., and Bruneau, M., 2001, Thermal wave harmonics generation in the hydrodynamical heat transport in thermoacoustics, *J. Acous. Soc. Am.*, **109**, pp. 84-90.
13. Besnoin, E., Numerical study of heat exchangers, 2001, PhD Thesis, The Johns Hopkins University, Baltimore.
14. Blanc-Benon, Ph., Besnoin, E., and Knio, O., 2003, Experimental and computational visualization of the flow field in a thermoacoustic stack, *C. R. Mecanique*, **331**, pp. 17-24.
15. Bogey, C. and Bailly, C., 2004, A family of low dispersive and low dissipative explicit schemes for flow and noise computations, *J. Comput. Phys.*, **194**, pp. 194--214.

**G.Penelet<sup>1</sup>, V.Gusev<sup>1,2</sup>, P.Lotton<sup>1</sup>, and M.Bruneau<sup>1</sup>**  
**EXPERIMENTAL AND THEORETICAL STUDIES OF NONLINEAR**  
**SATURATION PROCESSES IN ANNULAR THERMOACOUSTIC**  
**PRIME MOVERS**

<sup>1</sup>Laboratoire d'Acoustique de l'Université du Maine, UMR CNRS 6613

<sup>2</sup>Laboratoire de Physique de l'Etat Condensé, UMR CNRS 5509

Avenue Olivier Messiaen, 72085 Le Mans Cedex 9, France

Phone : (33) 243 83 36 26, Fax : (33) 243 83 35 20

E-mail : guillaume.penelet@univ-lemans.fr

*The present study gives a simplified analytical description of spontaneous generation and finite amplitude saturation of sound in annular thermoacoustic engines, and also provides comparison with experiments. The model includes the description of thermoacoustic amplification of sound (induced by interaction between an heterogeneously heated stack of solid plates and resonant gas oscillations), which accounts for the details of the temperature distribution in the whole thermoacoustic device. The saturation of the acoustic wave amplitude is described by taking into account both the reverse influence of the acoustic field on the temperature field, and the dissipation of acoustic power due to*